EDGE ARTICLE

Profiling single-molecule reaction kinetics under nanopore confinement†

Wei Liu,[a] Zhong-Lin Yang,[a] Chao-Nan Yang,[a] Yi-Lun Ying [ID] *[ab] and Yi-Tao Long [ID] [a]

The study of a single-molecule reaction under nanoconfinement is beneficial for understanding the reactive intermediates and reaction pathways. However, the kinetics model of the single-molecule reaction under confinement remains elusive. Herein we engineered an aerolysin nanopore reactor to elaborate the single-molecule reaction kinetics under nanoconfinement. By identifying the bond-forming and non-bond-forming events directly, a four-state kinetics model is proposed for the first time. Our results demonstrated that the single-molecule reaction kinetics inside a nanopore depends on the frequency of individual reactants captured and the fraction of effective collision inside the nanopore confined space. This insight will guide the design of confined nanopore reactors for resolving the single-molecule chemistry, and shed light on the mechanistic understanding of dynamic covalent chemistry inside confined systems such as supramolecular cages, coordination cages, and micelles.

Introduction

In nature, nanoconfinement is the key feature of the enzymatic reaction, where the substrates selectively encounter reactive sites.[1] The confined intermolecular interactions between enzymes and substrates facilitate the pre-organization of reagents, giving exceptional reaction efficiency. Inspired by enzyme confinement, reaction vessels at the micro/nanoscale are engineered to capture and organize the reagent, which is formed by nanoparticles,[2] micelles,[3] supramolecular cages,[4] coordination cages,[5] and proteins.[6–8] In this way, confined space is further designed to isolate a single reactant from the bulk, which is beneficial for studying the reactive intermediates and reaction pathways.

Biological nanopores utilize membrane proteins to form nanoconfinement for accommodating single molecules.[9–13] Reactive groups could be spatially designed alone in the polypeptide chain of a protein nanopore. Under bias voltages, a single reactant is confined inside a nanopore with controllable movement and direction. The covalent bond formation can be triggered at a specific reactive site, leading to the ionic current modulation through a nanopore.[14,15] Coupled with a high bandwidth current recording system, the nanopore could report reactive intermediates in real time,[16–18] study the reaction kinetics,[19–21] and explore reaction trajectory[22–24] at the single-molecule level.

Generally, the reaction between a single reactant molecule and reactive site inside a nanopore is proposed as a *pseudo* first order process.[25] Their reaction rate is calculated by a concentration-dependent experiment.[26] This kinetics model has also been expanded to study interactions between the transported analyte and the nanopore, including the electrostatic interaction between ssDNA and DNA polymerase,[27] the hydrophobic interaction between DNA and a graphene nanopore[28] and even the hydrogen bond of paired bases inside a nanopore.[29] Continuous efforts have been made to understand the contribution of driving force on the interaction kinetics under nanopore confinement.[30–33] But questions remain, for example, how does the driving force of the reactant affect the interaction kinetics? Why does the bulk concentration of the reactant affect the single-molecule reaction kinetics under nanopore confinement? How does the capture frequency regulate the reactive kinetics? In the enzyme-catalysis process, the reaction pathway is divided into the binding/unbinding of the substrate and the conversion of the reactant to a product, which is supported by the Michaelis–Menten equation. Inspired by this model,[34] we classify the single-molecule reaction process inside a nanopore into three steps which are (1) capture of a single reactant, (2) trigger of the single-molecule reaction at a specific site and (3) possible dissociation of the single reactant from the reactive site inside a nanopore. To profile the kinetics of this reaction, the rapid translocation of the single reactant should be slowed down to clearly record the above three processes.

Herein we designed a series of thiol-containing peptides (R_1–R_5) as reactants to bond with cysteine mutant aerolysin (AeL) nanopore. A previous study demonstrated that the cysteine

[a]*State Key Laboratory of Analytical Chemistry for Life Science, School of Chemistry and Chemical Engineering, Nanjing University, Nanjing, 210023, P. R. China. E-mail: yilunying@nju.edu.cn*

[b]*Chemistry and Biomedicine Innovation Center, Nanjing University, Nanjing, 210023, P. R. China*

mutants at the 238 site could prolong the residence of single molecules under nanoconfinement.[35] Therefore, K238C AeL was designed for simultaneously probing reaction events and non-reaction events, producing the distinguishable ionic current signatures. This model system ensures the study of the single-molecule reaction kinetics. Our results demonstrated that the reaction kinetics inside a nanopore depends on the reactant capture frequency and a fraction of effective collision between a single reactant and the active site under nanopore confinement.

Results and discussion

In the first step, a K238C AeL nanopore reactor with seven inward-facing cysteines at position 238 was employed to real-time monitor a disulfide formatting and breaking reaction (Fig. 1a). The constriction of AeL is around 1 nm and the length of the whole channel is approximated to 10 nm, which provides nanoconfinement for studying the single-molecule reaction.[36] The conductance of K238C AeL is 0.52 ± 0.02 nS in 1 M KCl ($n = 5$) at $20.0 \pm 2.0\ °C$ (Fig. S1 and S2†). Under the positive potential (*cis* side is grounded) from +60 mV to +120 mV, K238C AeL shows a stable open pore current with rare gating events.

The thiol derivative, thiol-containing peptide (**R**), is designed and contains a glutamic acid (E) segment as the guiding sequence at the N-terminal and a reactive cysteine at the C-terminal. We use **R₁** (EEESGSGSGSGSGSC) as a model reactant

to demonstrate our proposed kinetics model. The ionic events of **R₁** could be classified into type I for reaction events with long durations (>120 ms) and type II for non-reaction events with short durations. The bumping events were excluded from further analysis (Fig. S3–S5, see details in ESI 2.2†).

Both the reaction and non-reaction events were observed under the whole bias voltage ranging from +60 mV to +110 mV (with respect to the *cis* chamber, Fig. S6†). These results reveal that the single reactant could undergo either the reaction or non-reaction (translocation or bumping out) pathway as it approaches reactive site of the nanopore. Therefore, we proposed a four-state kinetic model to describe single-molecule reactions inside a nanopore as shown in Fig. 1a and eqn (1)–(3). When the reactant peptide (**R**) is confined into K238C AeL (**P**) from the *cis* side, it continuously moves and collides along the inner surface of K238C AeL under the bias voltage. Then, **R** reaches the reactive thiol groups at the 238 site, and interacts with the cysteine residues, giving an intermediate state of $[\mathbf{P}\cdots\mathbf{R}]^{\ddagger}$ (eqn (1)), similar to the enzyme–substrate binding. Due to the confinement effect, $[\mathbf{P}\cdots\mathbf{R}]^{\ddagger}$ acquires sufficient energy to enable the covalent bond formation, resulting in a disulfide product of **PR** (eqn (2)). This process of $\mathbf{P} + \mathbf{R} \rightarrow [\mathbf{P}\cdots\mathbf{R}]^{\ddagger} \rightarrow \mathbf{PR}$ yields reaction events. Alternatively, $[\mathbf{P}\cdots\mathbf{R}]^{\ddagger}$ would be dissociated after a rapid interaction but not form the bond with the K238C site (eqn (3)). If the driving force of **R** is larger than the repelling force from the translocation energy barrier, **R** translocates through the nanopore. Otherwise, **R** escapes from the *cis*
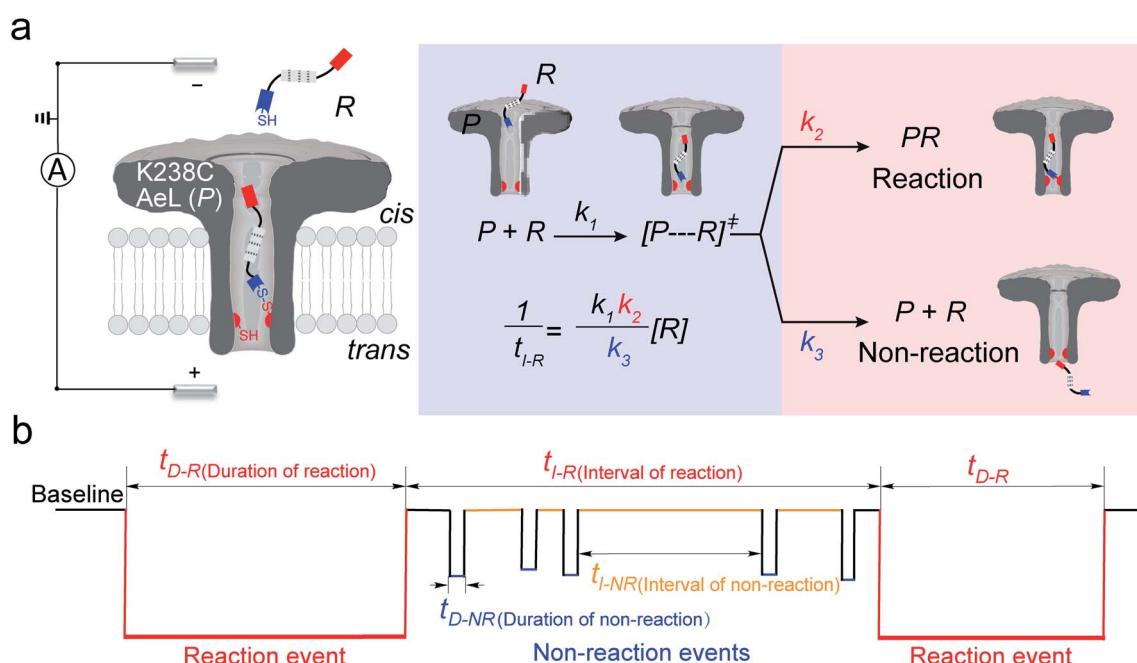
Fig. 1 (a) A schematic illustration of the single-molecule reaction between **R** and a K238C AeL nanopore (P); (b) the current trace model for the reaction event and non-reaction event. The kinetics model describes the four states: (1) capture of **R** into the nanopore, (2) energizing of a cysteine residue for $[\mathbf{P}\cdots\mathbf{R}]^{\ddagger}$ by the collision of **R** with the K238C site, (3) formation of a covalent bond between **R** and K238C, (4) release of **R** after deactivation. The non-reacted reactant escapes from K238C AeL either from the *cis* side or *trans* side. k_1, k_2 and k_3 represent the kinetics constant of each step. [R] refers to the concentration of the reactant. t_{I-R} stands for the time interval between adjacent reaction events. t_{I-NR} refers to the time interval between adjacent non-reaction events. t_{D-R} denotes the time duration of reaction events. t_{D-NR} denotes the time duration of non-reaction events.

side of the nanopore. The second pathway $\mathbf{P} + \mathbf{R} \rightarrow [\mathbf{P}\cdots\mathbf{R}]^{\ddagger} \rightarrow \mathbf{P} + \mathbf{R}$ generates non-reaction events.

$$\mathbf{P} + \mathbf{R} \xrightarrow{k_1} [\mathbf{P}\cdots\mathbf{R}]^{\ddagger} \tag{1}$$

$$[\mathbf{P}\cdots\mathbf{R}]^{\ddagger} \xrightarrow{k_2} \mathbf{PR} \tag{2}$$

$$[\mathbf{P}\cdots\mathbf{R}]^{\ddagger} \xrightarrow{k_3} \mathbf{P} + \mathbf{R} \tag{3}$$
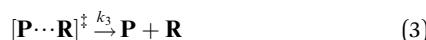
wherein k_1, k_2 and k_3 denote the rate constant of eqn (1), (2) and (3), respectively. As described in a previous study,[25] the reactant capture process inside a nanopore follows the *pseudo* first order process. This approximation assumes that the single reactant molecules are captured one-by-one in a nanopore. In our assay, each reactant cannot be simultaneously captured in a confined nanopore, which meets the assumption of the *pseudo* first order process (see details in ESI 2.2†). Then, k_1 is estimated by using eqn (4):

$$k_1 = \frac{1}{t_I[\mathbf{R}]} = \frac{f_{[\mathbf{P}\cdots\mathbf{R}]^{\ddagger}}}{[\mathbf{R}]} \approx \frac{f_{\mathbf{P}+\mathbf{R}}}{[\mathbf{R}]} = \frac{1}{t_{I\text{-}NR}[\mathbf{R}]} \tag{4}$$

where t_I refers to the time interval of all events (both reaction and non-reaction events, Fig. S7†), and $[\mathbf{R}]$ is the concentration of the reactant. $f_{[\mathbf{P}+\mathbf{R}]^{\ddagger}}$ and $f_{\mathbf{P}+\mathbf{R}}$ are the frequency of all captured events and non-reaction events, respectively. In order to understand the single-molecule reaction kinetics when the reactant was captured, we use the fraction of effective collision (ECF)[37] for describing the disulfide bond formation possibility inside K238C AeL as shown in eqn (5):

$$\text{ECF} = \frac{N_{\mathbf{PR}}}{N} = \frac{f_{\mathbf{PR}}}{f_{[\mathbf{P}\cdots\mathbf{R}]^{\ddagger}}} = \frac{t_I}{t_{I\text{-}R}} \times 100\% \tag{5}$$

where N refers to the number of captured $\mathbf{R}$, and $N_{\mathbf{PR}}$ represents the number of reaction events. Accordingly, $f_{\mathbf{PR}}$ is the reaction frequency of product $\mathbf{PR}$. The ECF can be calculated from the time interval between two adjacent reaction events ($t_{I\text{-}R}$) and t_I (Fig. S7†). Under high bias voltages (>+80 mV), the number of non-reaction events is thirteen times larger than reaction events of $\mathbf{R_1}$ (Table S1†). Therefore, the value of $t_{I\text{-}NR}$ is closer to that of t_I. eqn (5) could be simplified into eqn (6):

$$\text{ECF} = \frac{t_{I\text{-}NR}}{t_{I\text{-}R}} \times 100\% \tag{6}$$

According to the steady-state approximation,[37] the ECF can be expressed by the rate constant of two parallel reactions triggered by eqn (2) (k_2) and eqn (3) (k_3) as eqn (7):

$$\begin{aligned}\text{ECF} &= \frac{N_{\mathbf{PR}}}{N_{\mathbf{PR}} + N_{\mathbf{P}+\mathbf{R}}} = \frac{f_{\mathbf{PR}}}{f_{\mathbf{PR}} + f_{\mathbf{P}+\mathbf{R}}} \\ &= \frac{k_2 \times [\mathbf{P}\cdots\mathbf{R}]^{\ddagger}}{k_2 \times [\mathbf{P}\cdots\mathbf{R}]^{\ddagger} + k_3 \times [\mathbf{P}\cdots\mathbf{R}]^{\ddagger}} = \frac{k_2}{k_2 + k_3}\end{aligned} \tag{7}$$

wherein $N_{\mathbf{P}+\mathbf{R}}$ refers to the number of non-reaction events. When $N_{\mathbf{P}+\mathbf{R}} \gg N_{\mathbf{PR}}$ is at higher bias voltages, eqn (7) could be simplified into eqn (8):

$$\text{ECF} = \frac{k_2}{k_3} \times 100\% \tag{8}$$

Combining eqn (4)–(8), the single-molecule reaction rate under nanopore confinement could be calculated by using eqn (9) and (10) when the majority of reactants undergo the non-reaction pathway.

$$f_{\mathbf{PR}} = \frac{1}{t_{I\text{-}R}} = \text{ECF} \times f_{[\mathbf{P}\cdots\mathbf{R}]^{\ddagger}} = k_1\text{ECF}[\mathbf{R}] = \frac{k_1 k_2}{k_2 + k_3}[\mathbf{R}] \tag{9}$$

$$f_{\mathbf{PR}} = \frac{k_1 k_2}{k_3}[\mathbf{R}] \tag{10}$$

To verify the proposed kinetics we initially analyzed the frequency of reaction events at various concentrations. As expected, the ECF gives a constant value of $(17.0 \pm 2.0)\%$ while $f_{\mathbf{PR}}$ is linearly increased with the increase in the $[\mathbf{R_1}]$ concentration (Fig. 2a). These results demonstrate that the ECF is nearly irrelevant to the $\mathbf{R_1}$ concentration. The high possibility for effective trapping of $\mathbf{R_1}$, giving the high occurrence of formation of $[\mathbf{P}\cdots\mathbf{R_1}]$.

The results from voltage-dependent studies show that the higher voltage provides a larger k_1 due to the stronger driving force for the negatively charge $\mathbf{R_1}$ (Fig. S5b†). Consequently, $f_{\mathbf{PR}}$ gradually increases from +60 mV to +80 mV (Fig. 2b). However, $f_{\mathbf{PR}}$ does not show significant change at the bias voltage from +80 mV to +110 mV. When the bias voltage increased from +60 mV to +80 mV, the ECF showed a constant value of $(18.0 \pm 2.0)\%$ (Fig. 2b). Then, it decreased rapidly as the bias voltage exceeds the threshold of +80 mV. The low bias voltage (<+80 mV) is in favor of the formation pathway of the disulfide bond. However, the high bias voltage (>+80 mV) is prone to deactivation of $[\mathbf{P}\cdots\mathbf{R_1}]^{\ddagger}$ to release $\mathbf{R_1}$ from the *trans* side. At +110 mV, $f_{\mathbf{P}+\mathbf{R}}$ is over 100
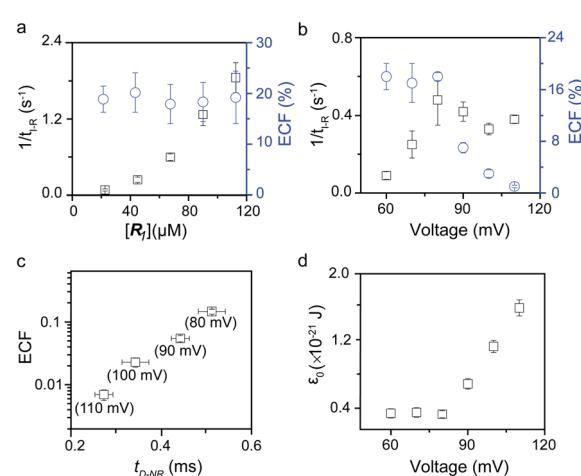

Fig. 2 Kinetics evaluation of $\mathbf{R_1}$ reacting with the K238C AeL nanopore. (a) The reaction rate ($f_{\mathbf{PR}} = 1/t_{I\text{-}R}$) and fraction of effective collision (ECF) at different $\mathbf{R_1}$ concentrations. (b) Reaction rate ($f_{\mathbf{PR}}$) and ECF under different voltages from +60 mV to +110 mV. (c) The relationship between the ECF and non-reaction event duration ($t_{D\text{-}NR}$). The voltage dependent results of $t_{D\text{-}NR}$ and $t_{I\text{-}NR}$ are shown in Fig. S5a and b,† respectively. (d) The collision threshold energy (ε_0) under different voltages from +60 mV to +110 mV. All data were acquired at $20.0 \pm 2.0\,^{\circ}C$ in 1.0 M KCl, 10.0 mM Tris, and 1.0 mM EDTA solution buffered at pH 8.0 in the presence of 50.0 μM $\mathbf{R_1}$.

times larger than f_{PR}, which suggests that most of the $\mathbf{R_1}$ molecules undergo ineffective bonding at a high bias voltage (Table S1†). In our four-state kinetics model, the reaction rate is controlled by the reactant captured and the result of two parallel reaction pathways of the process of eqn (2) and (3). At a defined temperature and pH, the reaction rate is mainly restricted by the process of eqn (3) rather than eqn (2). More interestingly, at a low voltage (<+80 mV), f_{PR} is increased from +60 mV to +80 mV, which is mainly dominated by the process of eqn (1). At a high voltage (>+80 mV), the destabilization of $[\mathbf{P}\cdots\mathbf{R_1}]^{\ddagger}$ significantly shifts the reaction pathway to the non-reaction pathway, thereby inhibiting the eqn (2) process.

We assume that k_3 is correlated with the velocity of $\mathbf{R_1}$ reaching and escaping from the 238 site. Our previous studies demonstrated that the 238 site is located at the energy barrier of the single-molecule translocation.[38] Compared with WT AeL, K238C prolongs the duration of poly(dA)$_4$ for about 7 times.[34] Therefore, K238C AeL could decrease the velocity of $\mathbf{R_1}$. The increasing residence time of single reactants at the reaction site can effectively improve the reaction efficiency. Moreover, the linear relationship between lg(ECF) and duration time of the

non-reaction event ($t_{D\text{-}NR}$) further supports our hypothesis (Fig. 2c).

The collision threshold energy (ε_0) between AeL and $\mathbf{R_1}$ can be calculated from the ECF for the formation of the disulfide bond under nanopore confinement according to the previous study[37] (eqn (11), see details in ESI 2.3†):

$$\varepsilon_0 = -\ln(\text{ECF})k_B T \tag{11}$$

wherein k_B is the Boltzmann constant and T is the experiment temperature (K). ε_0 changes with the bias voltage, as shown in Fig. 2d. The strong electrophoresis force facilitates the fast translocation of $\mathbf{R_1}$ with negative charges, which, in turn, significantly reduces effective collision possibility between $\mathbf{R_1}$ with the K238C site at high voltages. Only reactant molecules in the high energy state could induce the bond-formation process. Therefore the voltage could be effectively modulated for manipulating single-molecule reactions under nanopore confinement. In the above discussion, we clarified that the single-molecule reaction kinetics inside a nanopore is dominated by both f_{P+R} and ECF. f_{P+R} is associated with capture rate
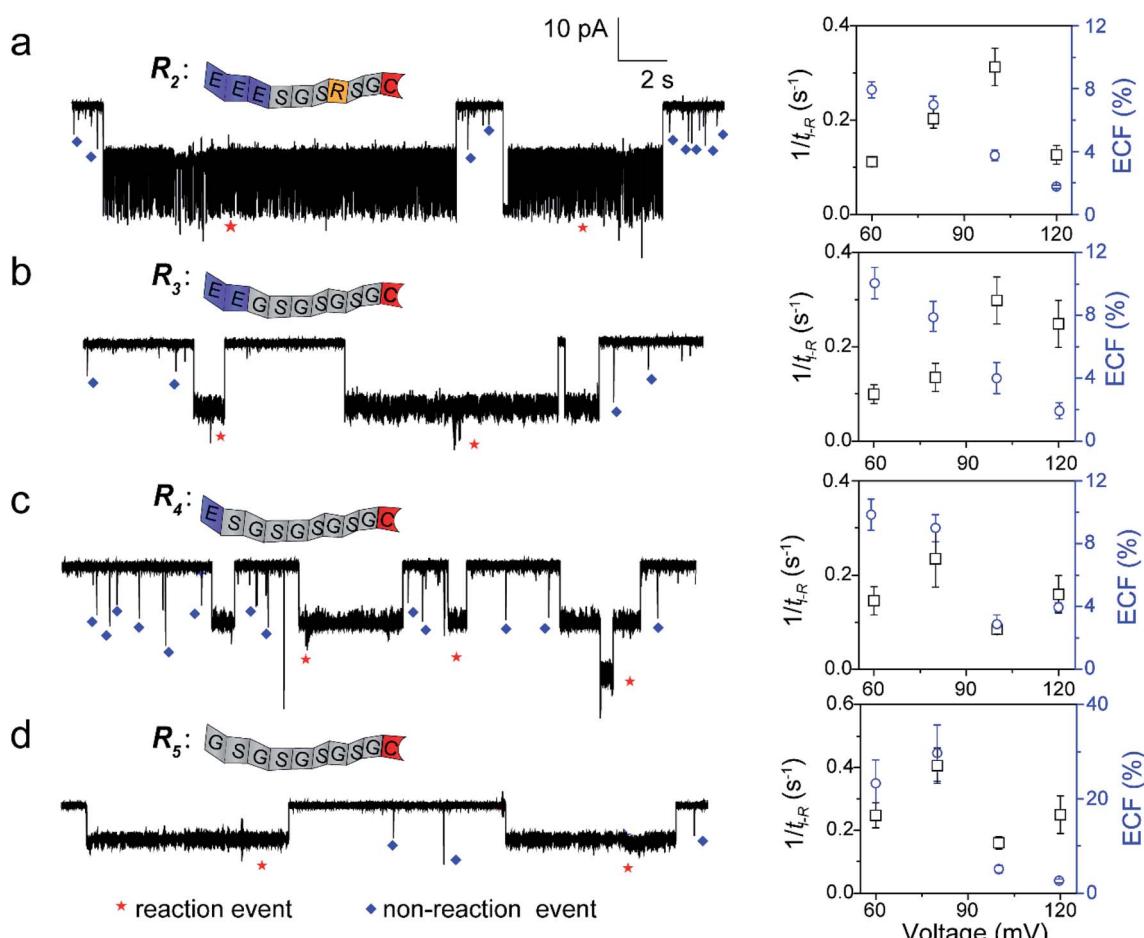
**Fig. 3** The single-molecule reaction of R_2 (a), R_3 (b), R_4 (c), and R_5 (d) with a K238C AeL nanopore. Left: the ionic current trace at +60 mV. The red and blue symbols represent the reaction events, and non-reaction events, respectively. Right: voltage dependent of the reaction rate ($f_{PR} = 1/t_{I\text{-}R}$) and ECF. The current fluctuation of the reaction events may be attributed to the conformational changes of the peptide or the possible intermediates. All data were acquired at 20.0 ± 2.0 °C in 1.0 M KCl, 10.0 mM Tris, and 1.0 mM EDTA solution buffered at pH 8.0 in the presence of 50.0 µM reactant. The short bumping events have been excluded.

constant k_1 and the bulk concentration of **R**. The ECF is determined by the bond active rate constant k_2 and deactivation rate constant of $[\mathbf{P}\cdots\mathbf{R_1}]^{\ddagger}$ (k_3).

To further confirm our kinetics model, we designed a series of cysteine-containing peptides. As shown in Fig. 3a and b, two peptides (**R₂** and **R₃**) exhibit the same length and same net charge but different charge distributions. Two types of events with a distinguishable duration difference are shown in Fig. S8a and b.† For **R₂** and **R₃**, $f_{\mathbf{PR}}$, ECF and the relationship between $t_{\mathrm{D\text{-}NR}}$ and the ECF show similar voltage-dependent tendencies (Fig. 3a, b, S10a and b†). Since both **R₂** and **R₃** carry two negative charges under pH 8.0, their k_1 values increase with increasing positive voltage (Fig. S8a and b†). At a voltage >+100 mV, the reaction rate is mainly affected by decreasing ECF. Note that the heterogeneous charge distribution of **R₂** and **R₃** affects the capture possibility and duration, resulting in the difference of k_1 and ECF (Table S1†).

For modulating the residence time, another two peptides, **R₄** and **R₅** were designed (Fig. 3c and d), which remove the one (**R₄**) and two (**R₅**) negatively charged amino acids from the guiding segment, respectively. As expected, the order of the ECF is **R₅** > **R₄** at the lower voltages (≤+80 mV). The uncharged **R₅** threads through the pore at the slowest rate of about 20.0 nm ms^{-1} compared with **R₃** and **R₄**, leading to the largest ECF (Fig. S10c, d, and Table S1†). For all the four peptides, their trends of $f_{\mathbf{PR}}$ in voltage are diverse and irregular, however, the voltage-dependent trends of the ECF are similar to that of **R₁**. The results confirm that the ECF is decreased with the enhanced translocation speed of non-reaction events at high voltages.

In our experiments, all reaction events could return to the initial open-pore state, illustrating that the disulfide bond could be cleaved without additional reducing agents under nanoconfinement. To analyze the single bond-breaking process, we prepared a three-state kinetics model for describing the disulfide bond breaking under nanopore confinement (Fig. S11†). The breaking of a single disulfide bond is divided into two steps: (1) $\mathbf{PR} \rightarrow [\mathbf{P}\cdots\mathbf{R}]^{\ddagger}$ for a single disulfide bond breaks down with a rate constant of $1/k_2$. (2) Then [**R**] escapes from the *trans* side of the pore, that is, $[\mathbf{P}\cdots\mathbf{R}]^{\ddagger} \rightarrow \mathbf{P} + \mathbf{R}$ gives a rate constant of k'_3. $1/t_{\mathrm{D\text{-}R}}$ could be calculated by using eqn (12):

$$\frac{1}{t_{\mathrm{D\text{-}R}}} = \frac{k'_3}{k_2} \tag{12}$$

wherein $1/t_{\mathrm{D\text{-}R}}$ is independent of the concentration of **R₁** (Fig. S11b†), which is consistent with the single-molecule dissociation process.[39] A high bias voltage (up to +110 mV) is prone to accelerating the translocation rate, which in term produces a small $t_{\mathrm{D\text{-}R}}$ for **R₁**–**R₅** (Fig. S11c†). These results are consistent with the previous study that the large extended force decreases the stability of disulfide bonds.[40] The logarithm of the bond stability constant ($1/t_{\mathrm{D\text{-}R}}$) of **R₁**–**R₅** shows an approximately linear relationship with the bias voltage. The slopes show a order of **R₁** > **R₂** ≈ **R₃** ≈ **R₅** > **R₄** (Fig. S11c†). The breaking of a disulfide bond between **R₄** and K238C is more tolerant at the bias voltage than the other four peptides due to the heterogeneous charge distribution at two terminals.

Conclusions

In conclusion, the nanopore confined effect provokes the "four-state kinetics module" for a single-molecule reaction. The kinetics of bond-forming is decided by both the possibility of the captured molecule ($k_1[\mathbf{R}]$) and fraction of effective collision (ECF) inside a nanopore. According to concentration and bias voltage-dependent experiments, the ECF is dominated by the bond active rate constant k_2 and deactivation rate constant of $[\mathbf{P}\cdots\mathbf{R}]^{\ddagger}$ (k_3). Moreover, the charge and composition effects could affect the values of $f_{\mathbf{P+R}}$ and ECF, leading to the differences of reaction constants. This reaction kinetics model provides a new basis for the design of nanopore reactors. We anticipate that this model could be extended to a wide range of organic and inorganic nanoconfinements for promoting multiple single-molecule reactions and interactions.

Data availability

All experimental supporting data and procedures are available in the ESI.†

Author contributions

YLY and YTL conceived the idea. WL and ZLY conducted the experiments and analysed the data. WL and CNY prepared the manuscript. WL and YLY wrote the manuscript.

Conflicts of interest

There are no conflicts to declare.

Acknowledgements

Notes and references

1 A. B. Grommet, M. Feller and R. Klajn, *Nat. Nanotechnol.*, 2020, **15**, 256–271.

2 T. Zdobinsky, P. S. Maiti and R. Klajn, *J. Am. Chem. Soc.*, 2014, **136**, 2711–2714.

3 J. Lee, D. Samanta, H. Nam and R. Zare, *J. Am. Chem. Soc.*, 2019, **141**, 10585–10589.

4 A. Palma, M. Artelsmair, G. Wu, X. Lu and O. A. Scherman, *Angew. Chem., Int. Ed.*, 2017, **129**, 15894–15898.

5 H. Takezawa, K. Shitozawa and M. Fujita, *Nat. Chem.*, 2020, **12**, 574–578.

6 S. Dutta, J. R. Whicher, D. A. Hansen, *et al.*, *Nature*, 2014, **510**, 512–517.

7 J. A. Mindell, H. J. Zhan, P. D. Huynh, R. J. Collier and A. P. Finkelstein, *Proc. Natl. Acad. Sci. U. S. A.*, 1994, **91**, 5272–5276.

8 Y. Qing, H. Tamagaki-Asahina, S. A. Ionescu, M. D. Liu and H. Bayley, *Nat. Nanotechnol.*, 2019, **14**, 1135–1142.

9 Y.-L. Ying and Y.-T. Long, *J. Am. Chem. Soc.*, 2019, **141**, 15720–15729.

10 L. Xue, H. Yamazaki, R. Ren, M. Wanunu, A. P. Ivanov and J. B. Edel, *Nat. Rev. Mater.*, 2020, **5**, 931–951.

11 N. S. Galenkamp, A. Biesemans and G. Maglia, *Nat. Chem.*, 2020, **12**, 481–488.

12 P. Tripathi, A. Benabbas, B. Mehrafrooz, H. Yamazaki and M. P. Wanunu, *Proc. Natl. Acad. Sci. U. S. A.*, 2021, **118**, 1–10.

13 L. Liu and H.-C. Wu, *Angew. Chem., Int. Ed.*, 2016, **55**, 15216–15220.

14 S. Shin, T. Luchian, S. Cheley, O. B. And and H. Bayley, *Angew. Chem., Int. Ed.*, 2002, **114**, 3859–3861.

15 K.-P. Qiu, T. P. Fato, B. Yuan and Y.-T. Long, *Small*, 2019, **15**, 1805426.

16 W. J. Ramsay, N. A. W. Bell, Y. Qing and H. Bayley, *J. Am. Chem. Soc.*, 2018, **140**, 17538–17546.

17 M. M. Haugland, S. Borsley, D. F. Cairns-Gibson, A. Elmi and S. L. Cockroft, *ACS Nano*, 2019, **13**, 4101–4110.

18 T. Luchian, S. H. Shin and H. Bayley, *Angew. Chem., Int. Ed.*, 2003, **42**, 1925–1929.

19 G. S. Pulcu, N. S. Galenkamp, Y. Qing, G. Gasparini, E. Mikhailova, S. Matile and H. Bayley, *J. Am. Chem. Soc.*, 2019, **141**, 12444–12447.

20 Y.-J. Qing, G. S. Pulcu, N. A. W. Bell and H. Bayley, *Angew. Chem., Int. Ed.*, 2018, **57**, 1218–1221.

21 Y.-J. Qing, S. A. Ionescu, G. S. Pulcu and H. Bayley, *Science*, 2018, **361**, 908–912.

22 M. B. Steffensen, D. Rotem and H. Bayley, *Nat. Chem.*, 2014, **6**, 604–608.

23 B. Zhou, Y. Wang, C. Cao, D. Li and Y.-T. Long, *Sci. China: Chem.*, 2018, **61**, 1385–1388.

24 J. Lee and H. Bayley, *Proc. Natl. Acad. Sci. U. S. A.*, 2015, **112**, 13768–13773.

25 L. Q. Gu, O. Braha, S. Conlan, S. Cheley and H. Bayley, *Nature*, 1999, **398**, 686–690.

26 H. Bayley, *Single Molecules and Nanotechnology, Single-molecule covalent chemistry in a protein nanoreactor*, 2008, ch. 10, pp. 251–277.

27 M. Palla, S. Punthambaker, B. Stranges, *et al.*, *ACS Nano*, 2020, **15**, 489–502.

28 S. Banerjee, J. Wilson, J. Shim, M. Shankla, E. A. Corbin, A. Aksimentiev and R. Bashir, *Adv. Funct. Mater.*, 2014, **25**, 936–946.

29 R. Hang, C. G. Cheyne, A. M. Fleming, C. J. Burrows and H. S. White, *J. Am. Chem. Soc.*, 2018, **140**, 5153–5160.

30 J. E. Reiner, J. J. Kasianowicz, B. J. Nablo and R. N. J. Turro, *Proc. Natl. Acad. Sci. U. S. A.*, 2010, **107**, 12080–12085.

31 B. Luan and A. Aksimentiev, *J. Phys.: Condens. Matter*, 2010, **22**, 454123.

32 B. Cressiot, A. Oukhaled, G. Patriarche, *et al.*, *ACS Nano*, 2012, **6**, 6236–6243.

33 M. Richard, T. Susana and K. Syma, *Nanomaterials*, 2015, **5**, 144–153.

34 X. Xie and H. Lu, *J. Biol. Chem.*, 1999, **274**, 15967–15970.

35 M.-Y. Li, Y.-Q. Wang, Y. Lu, Y.-L. Ying and Y.-T. Long, *Front. Chem.*, 2019, **7**, 258–264.

36 I. Iacovache, S. De Carlo, N. Cirauqui, M. D. Peraro, F. Goot and B. Zuber, *Nat. Commun.*, 2016, **7**, 12062.

37 S.-K. Upadhyay, *Chemical Kinetics and Reaction Dynamics, Theories of Reaction Rate*, 2007, ch. 4, pp. 83–89.

38 Y.-Q. Wang, C. Cao, Y.-L. Ying, S. Li, M. B. Wang, J. Huang and Y.-T. Long, *ACS Sens.*, 2018, **3**, 779–783.

39 S. Borsley, M. M. Haugland, S. Oldknow, *et al.*, *Chem*, 2019, **5**, 1275–1292.

40 A. Wiita, S. Ainavarapu, H. Huang and J. M. Fernandez, *Proc. Natl. Acad. Sci. U. S. A.*, 2006, **103**, 7222–7227.